

Ain Shams University

Faculty of Science



Applications of Integrated Geophysical Surveys in Delineating Groundwater Occurrences at Cairo-Bilbeis Region, East Nile Delta, Egypt

A Thesis submitted for the degree of Master of Science as a partial
fulfillment for the requirements of Master degree of Science in Applied
Geophysics

By

Mohamed Ibrahim Mohamed Ahmed
B.Sc. in Geophysics—Faculty of Science, 2011
Ain Shams University

To

Geophysics Department
Faculty of Science
Ain Shams University

Supervised by

Dr. Ahmad Muhammad Sobhy Ahmad Helaly

Associate Professor of Geophysics

Department of Geophysics - Faculty of Science - Ain Shams University

Dr. Azza Mahmoud Abd El Latif El-Rawy

Lecturer of Geophysics

Department of Geophysics - Faculty of Science - Ain Shams University

Cairo – 2016

Note

The present thesis is submitted to Faculty of Science, Ain Shams University in partial fulfillment for the requirements of the Master degree of Science in Geophysics.

Beside the research work materialized in this thesis, the candidate has attended ten postgraduate courses for one year in the following topics:

1. Geophysical field measurements
2. Numerical analysis and computer programming
3. Elastic wave theory
4. Seismic data acquisition
5. Seismic data processing
6. Seismic data interpretation
7. Seismology
8. Engineering seismology
9. Deep seismic sounding
10. Structure of the earth

He successfully passed the final examinations in these courses.

In fulfillment of the language requirement of the degree, he also passed the final examination of a course in the English language.

Prof. Dr. Salah El-Din Abdel-Wahab Mousa

Head of Geophysics Department

Acknowledgement

After thanks to Allah, I would like to thank my direct supervisors Dr. **Ahmad Muhammad Sobhy Ahmad Helaly**, Associate Professor of Geophysics, Faculty of Science, Ain Shams University, for his guidance and leading comments in this work and efforts.

I'm deeply thankful to Dr. **Azza Mahmoud Abd El-Latif El-Rawy**, Lectruer of Geophysics, Faculty of Science, Ain Shams University, for sharing me the idea of this study, her effort and leading comments in this work and reviewing the write up.

Also I'm deeply thanks to **Prof. Dr. Said Abdel- Maaboud Aly**, Professor of Geophysics, Faculty of Science, Ain Shams University, for his help, guidance and his effort.

I would like also to thank the **Geophysics Department**, Faculty of Science, Ain Shams University, **for** providing the instruments and I'm deeply thankful to everyone that helped me to finish my work.

Finally I dedicated this work to my family and I'm actually and totally thank them for their patience, support and encouragement.

Abstract

The study area is located at Cairo-Bilbeis Desert road, north-eastern part of Greater Cairo, the eastern part of the Nile Delta, Egypt. It is located between X-coordinates 350940 and 352171 meter easting and Y-coordinates 3349671 and 3350543 meter northing at Zone 36 UTM-coordinate system. The study area is mainly covered by Tertiary and Quaternary sediments. The exposed section varies in thickness which increases toward the Nile Delta recording more than 1000 m.

The main objective of this study is to delineate the groundwater occurrences based on the identification of the geological formations, geological structures and groundwater aquifers in the study area. The second objective is the use of modern geophysical method (seismoelectric method) which is sensitive to the presence of fluids. The third objective is the integration between the different geophysical methods which are the shallow seismic refraction tomography, geo-electric and seismoelectric for identifying how successful is; to use seismoelectric method, where it has not been used before in Egypt, by comparing the results of these geophysical methods in the study area. Finally the calculation of the near surface soil geotechnical parameters and dynamic characteristics.

Sixteen seismic refraction tomography profiles with 24 geophone with seven shot per each profile, 10 seismoelectric profiles with 24 dipole and pre-amplifier with three shots per each profile and finally three vertical electrical sounding with AB/2 500, 500 and 600 meter are the data acquired for this study.

Analysis and interpretation of the geophysical data indicates that there are two groundwater aquifers in the study area. The first aquifer consists of the Miocene sands and sandstone which is located at a depth of about 75-80 meter from the ground surface with an average thickness of about 38.3 meter and contains fresh water with low salinity. The second aquifer consists of the Oligocene sands which is located at a depth of about 195-200 meter from the ground surface but our measurements did not reach to its bottom. Finally by comparing between the seismic refraction tomography and geo-electric results with the seismoelectric method we found good matching between the results.

Keywords: groundwater aquifers, seismic refraction tomography, geo-electric, seismoelectric

Contents

<u>Subject</u>	<u>Page No.</u>
Acknowledgment.....	I
Abstract.....	II
Contents.....	III
List of Tables.....	V
List of Figures.....	VI
Chapter 1: INTRODUCTION.....	1
1.1 Introduction.....	1
1.2 Location of the Study Area.....	2
1.3 Problems of the Study.....	3
1.4 Objective of the study.....	3
1.5 Available Data	3
1.6 Previous work	4
1.7 Geology of the study area.....	7
1.7.1 Structural Setting and Tectonic.....	12
1.7.2 East Nile Delta Geologic History.....	14
Chapter 2: SEISMIC REFRACTION TOMOGRAPHY.....	16
2.1 Introduction.....	16
2.2 Seismic Refraction Theoretical Background.....	18
2.2.1 General Principles of Wave Travel.....	18
2.2.2 Snell's Law.....	19
2.2.3 Critical refraction.....	20
2.3 Seismic Refraction Tomography Theory.....	23
2.3.1 Seismic Refraction inversion.....	24
2.3.1.1 Seismic Refraction Tomography Inversion Process.....	24
2.3.1.2 Forward Modeling.....	25
2.4 Seismic Refraction Tomography Work Flow.....	27
2.4.1 Seismic Refraction Tomography Acquisition.....	27
2.4.2 Data Analysis and Interpretation.....	41
2.4.2.1 Data Processing.....	41
2.4.2.2 Seismic Refraction Tomography Interpretation Flow Chart	42
2.4.3 Seismic Refraction Tomography Velocity Models.....	48
2.4.3.1 Seismic Refraction Tomography Line 1.....	48
2.4.3.2 Seismic Refraction Tomography Line 2.....	53
2.4.3.3 Seismic Refraction Tomography Line 3.....	58
2.4.3.4 Seismic Refraction Tomography Line 4.....	63
2.4.3.5 Seismic Refraction Tomography Line 5.....	68
2.4.4 Mapping the Structural Features of the Study Area.....	73
2.4.4.1 Surface Topography Map.....	74

2.4.4.2 Structure Contour Maps.....	75
2.4.4.2.1 Structure Contour Map on Top Miocene Sand.....	75
2.4.4.2.2 Structure Contour Map on Top Miocene Dry Deposits (upper part)	75
2.4.4.2.3 Structure Contour Map on Top Miocene Dry Deposits (lower part)	76
2.4.4.2.4 Structure Contour Map on Top Miocene Aquifer.....	77
2.4.4.3 3D Structural Model.....	78
2.4.4.4 3D Stratigraphic Model.....	81
2.5 Structural Regime of the Study Area	82
Chapter 3: DC ELECTRICAL RESISTIVITY.....	84
3.1 Introduction.....	84
3.2 Theory and Basic Principles.....	86
3.2.1 True Resistivity.....	86
3.2.2 Current Flow in a Homogeneous Earth.....	90
3.3 Electrode Configurations Used in Resistivity Method	92
3.3.1 Wenner Array.....	93
3.3.2 Schlumberger Array.....	94
3.3.3 Dipole-dipole Array.....	95
3.4 Vertical Electrical Sounding Data Measurements in the Study Area.....	96
3.5 Data Analysis and Interpretation.....	105
Chapter 4: SEISMOELECTRIC AND FINAL MODEL.....	112
4.1 Introduction.....	112
4.2 Theoretical Background.....	113
4.3 Seismoelectric Work Flow.....	119
4.3.1 Seismoelectric Data Acquisition.....	119
4.3.2 Seismoelectric Data Processing.....	123
4.4 Seismoelectric Data Interpretation.....	130
4.5 Comparison between the Results of the Used Geophysical Methods.....	142
Chapter 5: MULTICHANNEL ANALYSIS OF SURFACE WAVES (MASW) TECHNIQUE.....	144
5.1 Introduction.....	144
5.2 Multichannel Analysis of Surface Waves (MASW) Technique.....	145
5.3 Data Analysis and Interpretation.....	148
5.4 Geotechnical Parameters and Dynamic Characteristics.....	152
5.5 RESULTS.....	156
Chapter 6: Summary and Conclusions	160
References.....	168
Arabic Summary.....	

List of Tables

<u>Table Title</u>	<u>Page No.</u>
Table (2-1): Initial smoothed model parameters for line1.	48
Table (2-2): Initial layered model parameters for line1.	50
Table (2-3): layers parameters for line 1.	51
Table (2-4): Initial smoothed model parameters for line 2.	53
Table (2-5): Initial layered model parameters for line 2.	55
Table (2-6): Layers parameters for line 2.	56
Table (2-7): Initial smoothed model parameters for line 3.	58
Table (2-8): Initial layered model parameters for line 3.	60
Table (2-9): Layers parameters for line 3.	61
Table (2-10): Initial smoothed model parameters for line 4.	63
Table (2-11): Initial layered model parameters for line 4.	65
Table (2-12): Layers parameters for line 4.	66
Table (2-13): Initial smoothed model parameters for line 5.	68
Table (2-14): Initial layered model parameters for line 5.	70
Table (2-15): Layers parameters for line 5.	71
Table (3-1): VES#1 Data Sheet.	102
Table (3-2): VES#2 Data Sheet.	103
Table (3-3): VES#3 Data Sheet.	104
Table (3-4): True resistivities and thicknesses for the geo-electric layers calculated from the inverted apparent resistivity models.	106
Table (3-5): Average true resistivities and average thicknesses for eight interpreted geo-electrical layers in the study area.	108
Table (3-6): Geological layers and its corresponding average thickness found in the study area.	110
Table (4-1): Seismoelectric events depth calculation.	131
Table (5-1): Site classification scheme of NEHRP provisions (2003).	155
Table (5-2): Geotechnical Parameters and Dynamic Characteristics of layer 1.	156
Table (5-3): Geotechnical Parameters and Dynamic Characteristics of layer 2.	157
Table (5-4): Geotechnical Parameters and Dynamic Characteristics of layer 3.	157

List of Figures

<u>Figure Title</u>	<u>Page No.</u>
Figure (1-1): Location map of the study area.	2
Figure (1-2): Gravity maps, (a) Bouguer anomaly map, (b) Regional gravity anomaly map and (c) residual gravity map.	5
Figure (1-3): Fault elements dissecting the area from gravity interpretation.	6
Figure (1-4): Location map of the measured magnetic profiles (P1-P1`) and (P2-P2`).	6
Figure (1-5): 2D magnetic modeling.	7
Figure (1-6): Geological map of the study area.	8
Figure (1-7): Generalized stratigraphic column of the study area	10
Figure (1-8): Geological log from the Inshas borehole drilled by EGSMA	11
Figure (1-9): compiled structure map of the area east of the Nile Delta.	12
Figure (1-10): Structural zones of the east of the Nile Delta region	13
Figure (2-1): Schematic diagram of wave's propagation from the seismic source through the ground mediums.	19
Figure (2- 2): Snell's law schematic diagram.	20
Figure (2-3): Critical refraction at a plane boundary and the generation of a head wave.	21
Figure (2-4): Seismic refraction geometry.	22
Figure (2-5): Division of the model function into discrete cells and definition the ray-path with respect to position vector (r).	27
Figure (2-6): OYO McSeisSX24 multi-channel Seismograph.	28
Figure (2-7): Shot point location map.	29
Figure (2-8): Seismic Refraction Tomography array design.	30
Figure (2-9a): Field photos during the seismic refraction tomography data acquisition.	31
Figure (2-9b): Field photos during the seismic refraction tomography data acquisition.	31
Figure (2-9c): Field photos during the seismic refraction tomography data acquisition.	32
Figure (2-9d): Field photos during the seismic refraction tomography data acquisition	32
Figure (2-10): Shot records of profile 1, line 1.	33
Figure (2-11): Shot records of profile 2, line 1.	34
Figure (2-12): Shot records of profile 3, line 1.	34
Figure (2-13): Shot records of profile 4, line 1.	35
Figure (2-14): Shot records of profile 5, line 2.	35
Figure (2-15): Shot records of profile 6, line 2.	36
Figure (2-16): Shot records of profile 7, line 2.	36
Figure (2-17): Shot records of profile 8, line 3.	37
Figure (2-18): Shot records of profile 9, line 3.	37

Figure (2-19): Shot records of profile 10, line 3.	38
Figure (2-20): Shot records of profile 11, line 4.	38
Figure (2-21): Shot records of profile 12, line 4.	39
Figure (2-22): Shot records of profile 13, line 4.	39
Figure (2-23): Shot records of profile 14, line 5.	40
Figure (2-24): Shot records of profile 15, line 5.	40
Figure (2-25): Shot records of profile 16, line 5.	41
Figure (2-26): Filtering processes steps where (A) Raw Data , (B) After High Pass Filter and (C) After Low Pass Filter.	42
Figure (2-27): Zond2DST seismic refraction tomography flow chart.	44
Figure (2-28): Picking of the first arrival times, line 2 – Profile 4 – Normal Shot.	44
Figure (2-29): Picking of the first arrival times, line 5 – Profile 15.	45
Figure (2-30): Shot record of Normal Shot of profile 10 located at line 3	46
Figure (2-31): Travel time curves for the survey seismic lines.	47
Figure (2-32): Line 1 results, (A); travel-time curves, (B); smoothed velocity model, (C); layered velocity model, (D); relative sensitivity model, (E); DOI model and (F); geologic cross-section.	49
Figure (2-33): Line 2 results, (A); travel-time curves, (B); smoothed velocity model, (C); layered velocity model, (D); relative sensitivity model, (E); DOI model and (F); geologic cross-section.	54
Figure (2-34): Line 3 results, (A); travel-time curves, (B); smoothed velocity model, (C); layered velocity model, (D); relative sensitivity model, (E); DOI model and (F); geologic cross-section.	59
Figure (2-35): Line 4 results, (A); travel-time curves, (B); smoothed velocity model, (C); layered velocity model, (D); relative sensitivity model, (E); DOI model and (F); geologic cross-section.	64
Figure (2-36): Line 5 results, (A); travel-time curves, (B); smoothed velocity model, (C); layered velocity model, (D); relative sensitivity model, (E); DOI model and (F); geologic cross-section.	69
Figure (2-37): Surface topography of the survey area.	74
Figure (2-38): Structure contour map of top Miocene Sand.	75
Figure (2-39): Structure contour map of top Miocene dry deposits (upper part).	76
Figure (2-40): Structure contour map of top Miocene dry deposits (lower part).	77
Figure (2-41): Structure contour map of top Miocene aquifer.	78
Figure (2-42): 3D surfaces view with different color scale of the surface topography and subsurface geological layers seated in the study area.	79
Figure (2-43): 3D surfaces view with the same color scales of the surface topography and subsurface geological layers seated in the study area.	80
Figure (2-44): 3D surface elevation model for the survey area.	81
Figure (2-45): 3D stratigraphic model for the survey area.	82
Figure (2-46): Structure map for the survey area.	83
Figure (3-1): (A) Basic definition of resistivity across a homogeneous block of side length L with an applied current I and potential drop between	

opposite faces of V . (B) The electrical circuit equivalent, where R is a resistor.	87
Figure (3-2): Three extreme structures involving two materials with true resistivities ρ_1 and ρ_2 .	88
Figure (3-3): (A) Three-dimensional representation of a hemispherical equipotential shell around a point electrode on a semi-infinite, homogeneous medium. (B) Potential decay away from the point electrode.	90
Figure (3-4): Cross-section of current “tubes” and equipotential surfaces between a source and sink; numbers on the current lines indicate the fraction of current flowing above the line.	92
Figure (3-5): General four-electrode configuration for resistivity measurement, consisting of a pair of current electrodes (A, B) and a pair of potential electrodes (M, N).	93
Figure (3-6): Geometries of current and potential electrodes for Wenner Array.	94
Figure (3-7): Geometries of current and potential electrodes for Schlumberger Array.	95
Figure (3-8): Geometries of current and potential electrodes for Dipole-dipole Array.	96
Figure (3-9): Vertical electrical sounding field acquisition procedure using Schlumberger electrode configuration array, where M&N is the potential electrodes and A&B is the current electrodes.	97
Figure (3-10): ABEM Terrameter SAS 300 resistivity meter.	98
Figure (3-11): Field photo during the vertical electrical sounding data measurements.	99
Figure (3-12): Field photo during the vertical electrical sounding data measurements.	99
Figure (3-13): Field photo during the vertical electrical sounding data measurements.	100
Figure (3-14): Field photo during the vertical electrical sounding data measurements.	100
Figure (3-15): layout of the three VES's 1, 2 and 3 through the study area.	101
Figure (3-16): VES#1 measured and calculated apparent resistivity models.	106
Figure (3-17): VES#2 measured and calculated apparent resistivity models.	107
Figure (3-18): VES#3 measured and calculated apparent resistivity models.	107
Figure (3-19): Apparent resistivity section passing through the three VES's.	108
Figure (3-20): True resistivity section passing through the three VES's.	109
Figure (3-21): Geologic cross-section passing through the three VES's.	111
Figure (3-22): Inferred structure map of the study area with the seismic refraction tomography and geo-electric VES's locations.	111
Figure (4-1): Seismoelectric phenomena depend on the charge separation created by streaming currents that flow in response to the pressure gradient of a seismic wave. The electric double layer is responsible for streaming currents at the grain scale.	114
Figure (4-2): Two types of seismoelectric phenomena commonly measured in the field: (a) the co-seismic field of a P-wave (due to the charge	

accumulations “+” and “-”) and (b) the interface response created when the P-wave hits an interface at depth.	115
Figure (4-3): Schematic representation of the seismoelectric direct field.	117
Figure (4-4): Cartoon schematic of a “standard” in-line geometry seismoelectric survey and simple synthetic data.	119
Figure (4-5): Local differential pre-amplifiers.	120
Figure (4-6): Seismoelectric field acquisition photo.	121
Figure (4-7): Seismoelectric shot point location map.	122
Figure (4-8): Seismoelectric profile array design.	123
Figure (4-9): Line 4 – Profile 2 – Middle Shot, where a) Raw Seismoelectric record and b) Its Amplitude Spectrum.	125
Figure (4-10): Removal of the powerline harmonics (after Butler and Russel, 1993).	126
Figure (4-11): Removal of the powerline harmonic 50 Hz by using the band reject Butterworth filter for 50 Hz.	127
Figure (4-12): Line 4 – Profile 2 – Middle Shot, where a) Seismoelectric record after removal of the powerline harmonic 50 Hz and its harmonics and b) Amplitude Spectrum after removal of the powerline harmonic 50 Hz. and its harmonics.	127
Figure (4-13): Line 4 – Profile 2 – Middle Shot, where a) Seismoelectric record after applying the band bass filtering between (160-600 Hz) with polarity reversal around the shot point location and b) Amplitude Spectrum after applying the band bass filtering between (160-600 Hz).	128
Figure (4-14): Line 4 – Profile 2 – Middle Shot, where a) Seismoelectric record after applying the band bass filtering between (160-600 Hz) with same polarity around the shot location and b) Amplitude Spectrum after applying the band bass filtering between (160-600 Hz).	129
Figure (4-15): Line 2 – middle seismoelectric record with Inshas borehole where the seismoelectric events correlated to their corresponding boundaries at the Inshas borehole geological log.	130
Figure (4-16): Line 2 – Normal Seismoelectric Record, where a) processed seismoelectric record with interpreted seismoelectric events b) Amplitude Spectrum.	133
Figure (4-17): Line 2 – Middle Seismoelectric Record, where a) processed seismoelectric record with interpreted seismoelectric events b) Amplitude Spectrum.	134
Figure (4-18): Line 2 – Reverse Seismoelectric Record, where a) processed seismoelectric record with interpreted seismoelectric events b) Amplitude Spectrum.	135
Figure (4-19): Line 3 – Normal Seismoelectric Record, where a) processed seismoelectric record with interpreted seismoelectric events b) Amplitude Spectrum.	136
Figure (4-20): Line 3 – Middle Seismoelectric Record, where a) processed seismoelectric record with interpreted seismoelectric events b) Amplitude Spectrum.	137

Figure (4-21): Line 3 – Reverse Seismoelectric Record, where a) processed seismoelectric record with interpreted seismoelectric events b) Amplitude Spectrum.	138
Figure (4-22): Line 4 – Normal Seismoelectric Record, where a) processed seismoelectric record with interpreted seismoelectric events b) Amplitude Spectrum.	139
Figure (4-23): Line 4 – Middle Seismoelectric Record, where a) processed seismo-electric record with interpreted seismoelectric events b) Amplitude Spectrum.	140
Figure (4-24): Line 4 – Reverse Seismoelectric Record, where a) processed seismoelectric record with interpreted seismoelectric events b) Amplitude Spectrum.	141
Figure (4-25): Final model of the three used geophysical methods in the study.	143
Figure (5-1): A schematic of a typical MASW survey configuration.	146
Figure (5-2): A 3-step scheme for MASW data processing illustrated by an actual field data set.	148
Figure (5-3): Dispersion curve generation.	149
Figure (5-4): 2D Inversion of shear wave velocity model for line 2.	149
Figure (5-5): Line 1 velocity models where (A), Compressional wave (V_p) velocity model and (B), Shear wave (V_s) velocity model.	150
Figure (5-6): Line 2 velocity models where (A), Compressional wave (V_p) velocity model and (B), Shear wave (V_s) velocity model.	150
Figure (5-7): Line 3 velocity models where (A), Compressional wave (V_p) velocity model and (B), Shear wave (V_s) velocity model.	151
Figure (5-8): Line 4 velocity models where (A), Compressional wave (V_p) velocity model and (B), Shear wave (V_s) velocity model.	151
Figure (5-9): Line 5 velocity models where (A), Compressional wave (V_p) velocity model and (B), Shear wave (V_s) velocity model.	152
Figure (5-10): Relationship between the compressional wave velocity (V_p) and shear wave velocity (V_s) for the soil layers present in the study area.	159

CHAPTER ONE

INTRODUCTION

1.1 Introduction

Recently, due to the difficulties and challenges which Egypt faces especially in the diminishing of fresh water resources (where the Nile River water is insufficient to meet the demand of the Egyptians); as a result of the population growth, as well as the necessity of increasing the area of farmland and land reclamation. So, we must start in reliance on other sources of waters instead of the Nile River water. One of them is underground water which is the second source of fresh water in Egypt and could help partly in providing large quantities of fresh water. Groundwater is considered as one of the main sources of water, particularly in the desert regions.

The conventional method to determine the hydrological and geological situation of a site is to drill boreholes to bedrock. Applied geophysics will reduce the number of drill-holes required and attain detailed information on the hydrological and geological system. By mapping geologic structures with geophysical surveys, major saving can be made for cost and time.

The characterization of the subsurface requires a detailed knowledge of several properties of the composing rocks and fluids. Whereas some of these properties can be measured directly (by seismic and borehole methods), other properties have to be estimated by indirect measurement methods such as resistivity, time-domain electromagnetic (TEM), and magnetic (Bery, 2012).

The tasks for the geophysical investigations were the structural exploration of the groundwater and the closing of information gaps of the geological and hydrogeological exploration. Geophysical methods can give a continuous overview about the water bearing aquifers (the thickness and the depth below the surface, the size,... etc.). Furthermore, it is possible to detect additional aquifer layers in the underground (Schicht et al., 2013).

1.2 Location of the Study Area

The study area lies within the northeastern part of Greater Cairo (Egypt) at the Eastern part of the Nile Delta. It is located between X-coordinates 350940 and 352171 meter easting and Y-coordinates 3349671 and 3350543 meter northing at Zone 36 UTM-coordinate system as shown in Figure (1-1).

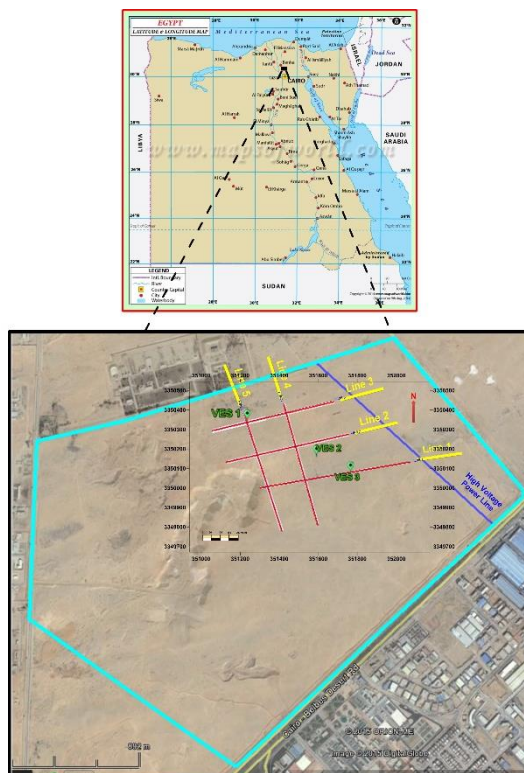


Figure (1-1): Location map of the study area.

1.3 Problem of the Study

In light of the above, the study problem can be determined through the following questions:

- 1) What is the probability of the presence of the groundwater in the study area?
- 2) How successful is the use of modern geophysical method; the seismoelectric method in determining groundwater occurrence and geological structures?
- 3) Suitability of groundwater well design according to the near-surface soil geotechnical parameters and dynamic characteristics.

1.4 Objectives of the Study

- 1) Identification of the geological formations, geological structures and groundwater aquifers in the study area based on interpretation models of seismic refraction tomography, geo-electric resistivity, and seismoelectric methods.
- 2) Integration between different geophysical methods; seismic refraction tomography, geoelectric resistivity and new geophysical method (seismoelectric).
- 3) Calculation of the near-surface soil geotechnical parameters and dynamic characteristics.

1.5 Available Data

Three different geophysical methods were chosen for underground water investigation of this study.

First, the seismic refraction tomography is used to give a good overview of the structure of the brine zone. Sixteen seismic refraction tomography profiles along five seismic lines with a total 112 shot record